

# Interferometric velocity measurements through a fluctuating gas-liquid interface employing adaptive optics

Lars Büttner,\* Christoph Leithold, and Jürgen Czarske

Technische Universität Dresden, Faculty of Electrical and Computer Engineering, Laboratory for Measurement and Testing Techniques, Helmholtzstraße 18, 01069 Dresden, Germany

\*Lars.Buettner@tu-dresden.de

[www.lasermetrology.de](http://www.lasermetrology.de)

**Abstract:** Optical transmission through fluctuating interfaces of mediums with different refractive indexes is limited by the occurring distortions. Temporal fluctuations of such distortions deteriorate optical measurements. In order to overcome this shortcoming we propose the use of adaptive optics. For the first time, an interferometric velocity measurement technique with embedded adaptive optics is presented for flow velocity measurements through a fluctuating air-water interface. A low order distortion correction technique using a fast deformable mirror and a Hartmann-Shack camera with high frame rate is employed. The obtained high control bandwidth enables precise measurements also at fast fluctuating media interfaces. This methodology paves the way for several kinds of optical flow measurements in various complex environments.

©2013 Optical Society of America

**OCIS codes:** (110.1080) Active or adaptive optics; (120.0120) Instrumentation, measurement, and metrology; (120.1088) Adaptive interferometry; (170.3340) Laser Doppler velocimetry; (230.6120) Spatial light modulators; (350.4600) Optical engineering.

---

## References and links

1. H. W. Babcock, "The possibility of compensating astronomical seeing," *Publ. Astron. Soc. Pac.* **65**(386), 229–236 (1953).
2. J. W. Hardy, *Adaptive Optics for Astronomical Telescopes* (Oxford University, 1998).
3. R. Davies and M. Kasper, "Adaptive optics for astronomy," *Annu. Rev. Astrophys.* **50**, arXiv:1201.5741 (2012).
4. J. Liang, D. R. Williams, and D. T. Miller, "Supernormal vision and high-resolution retinal imaging through adaptive optics," *J. Opt. Soc. Am. A* **14**(11), 2884–2892 (1997).
5. J. Rha, R. S. Jonnal, K. E. Thorn, J. Qu, Y. Zhang, and D. T. Miller, "Adaptive optics flood-illumination camera for high speed retinal imaging," *Opt. Express* **14**(10), 4552–4569 (2006).
6. A. Roorda, F. Romero-Borja, W. Donnelly Iii, H. Queener, T. J. Hebert, and M. C. W. Campbell, "Adaptive optics scanning laser ophthalmoscopy," *Opt. Express* **10**(9), 405–412 (2002).
7. R. J. Zawadzki, S. M. Jones, S. S. Olivier, M. Zhao, B. A. Bower, J. A. Izatt, S. Choi, S. Laut, and J. S. Werner, "Adaptive-optics optical coherence tomography for high-resolution and high-speed 3D retinal in vivo imaging," *Opt. Express* **13**(21), 8532–8546 (2005).
8. Y. Zhang, B. Cense, J. Rha, R. S. Jonnal, W. Gao, R. J. Zawadzki, J. S. Werner, S. Jones, S. Olivier, and D. T. Miller, "High-speed volumetric imaging of cone photoreceptors with adaptive optics spectral-domain optical coherence tomography," *Opt. Express* **14**(10), 4380–4394 (2006).
9. X. Xu, H. Liu, and L. V. Wang, "Time-reversed ultrasonically encoded optical focusing into scattering media," *Nat. Photonics* **5**(3), 154–157 (2011).
10. X. Tao, O. Azucena, M. Fu, Y. Zuo, D. C. Chen, and J. Kubby, "Adaptive optics microscopy with direct wavefront sensing using fluorescent protein guide stars," *Opt. Lett.* **36**(17), 3389–3391 (2011).
11. K. Si, R. Fiolka, and M. Cui, "Fluorescence imaging beyond the ballistic regime by ultrasound pulse guided digital phase conjugation," *Nat. Photonics* **6**(10), 657–661 (2012).
12. Y. M. Wang, B. Judkewitz, C. A. Dimarzio, and C. Yang, "Deep-tissue focal fluorescence imaging with digitally time-reversed ultrasound-encoded light," *Nat Commun* **3**, 928 (2012).
13. A. P. Mosk, A. Lagendijk, G. Lerosey, and M. Fink, "Controlling waves in space and time for imaging and focusing in complex media," *Nat. Photonics* **6**(5), 283–292 (2012).
14. B. Judkewitz, Y. M. Wang, R. Horstmeyer, A. Mathy, and C. Yang, "Speckle-scale focusing in the diffusive regime with time-reversal of variance-encoded light (TROVE)," *Nat. Photonics* **7**(4), 300–305 (2013).
15. T. R. Hillman, T. Yamauchi, W. Choi, R. R. Dasari, M. S. Feld, Y. Park, and Z. Yaqoob, "Digital optical phase conjugation for delivering two-dimensional images through turbid media," *Sci Rep* **3**, 1909 (2013).

16. R. Fiolka, K. Si, and M. Cui, "Complex wavefront corrections for deep tissue focusing using low coherence backscattered light," *Opt. Express* **20**(15), 16532–16543 (2012).
17. J. Jang, J. Lim, H. Yu, H. Choi, J. Ha, J. H. Park, W. Y. Oh, W. Jang, S. D. Lee, and Y. K. Park, "Complex wavefront shaping for optimal depth-selective focusing in optical coherence tomography," *Opt. Express* **21**(3), 2890–2902 (2013).
18. B. Böhm, C. Heeger, R. L. Gordon, and A. Dreizler, "New Perspectives on Turbulent Combustion: Multi-Parameter High-Speed Planar Laser Diagnostics," *Flow Turbul. Combust.* **86**(3–4), 313–341 (2010).
19. G. E. Elsinga, B. W. van Oudheusden, and F. Scarano, "Evaluation of aero-optical distortion effects in PIV," *Exp. Fluids* **39**(2), 246–256 (2005).
20. J. König, K. Tschulik, L. Büttner, M. Uhlemann, and J. Czarke, "Analysis of the Electrolyte Convection inside the Concentration Boundary Layer during Structured Electrodeposition of Copper in High Magnetic Gradient Fields," *Anal. Chem.* **85**(6), 3087–3094 (2013).
21. M. Neumann, C. Friedrich, J. Czarke, J. Kriegseis, and S. Grundmann, "Determination of the phase-resolved body force produced by a dielectric barrier discharge plasma actuator," *J. Phys. D Appl. Phys.* **46**(4), 042001 (2013).
22. G. Gomit, L. Chatellier, D. Calluud, and L. David, "Free surface measurement by stereo-refraction," *Exp. Fluids* **54**(6), 1540 (2013).
23. E. Schleicher, M. J. da Silva, S. Thiele, A. Li, E. Wollrab, and U. Hampel, "Design of an optical tomograph for the investigation of single- and two-phase pipe flows," *Meas. Sci. Technol.* **19**(9), 094006 (2008).
24. S. B. G. O'Brien and L. W. Schwartz, "Theory and modeling of thin film flows," in *Encyclopedia of Surface and Colloid Science* (Taylor and Francis, 2002), pp. 5283–5297.
25. S. Kalliadasis, C. Ruyer-Quil, B. Scheid, and M. G. Velarde, *Falling Liquid Films* (Springer, 2012).
26. P. C. Miles, "Geometry of the fringe field formed in the intersection of two Gaussian beams," *Appl. Opt.* **35**(30), 5887–5895 (1996).
27. J. Czarke, L. Büttner, T. Razik, and H. Müller, "Boundary layer velocity measurements by a laser Doppler profile sensor with micrometre spatial resolution," *Meas. Sci. Technol.* **13**(12), 1979–1989 (2002).
28. A. Sommerfeld, *Mechanics of Deformable Bodies (Lectures on Theoretical Physics)* (Academic, 1950).
29. R. K. Tyson, *Principles of Adaptive Optics*, 3rd ed. (CRC, 2010).
30. G. Vdovin and P. M. Sarro, "Flexible mirror micromachined in silicon," *Appl. Opt.* **34**(16), 2968–2972 (1995).
31. K.-H. Brenner and W. Singer, "Light propagation through microlenses: a new simulation method," *Appl. Opt.* **32**(26), 4984–4988 (1993).
32. K. Matsushima, H. Schimmel, and F. Wyrowski, "Fast calculation method for optical diffraction on tilted planes by use of the angular spectrum of plane waves," *J. Opt. Soc. Am. A* **20**(9), 1755–1762 (2003).

## 1. Introduction

Adaptive optics (AO) is predominantly known from astronomy, where it has led to a renaissance of large earth-bound telescopes [1–3]. Optical distortions of the light path through the atmosphere caused by turbulent flows can be corrected such that the resolution gets improved until the diffraction limit. Besides astronomy, adaptive optics has found its way into various fields of research. In ophthalmology, the integration of adaptive optics has improved the imaging of the retina as aberrations of the eye can be corrected [4–6]. Three dimensional in-vivo retinal imaging is possible by optical coherence tomography using AO [7, 8]. In latest developments, AO has been applied for digital optical phase conjugation to allow for imaging in highly scattering turbid media [9–17]. In order to achieve non-invasive focussing inside the turbid medium, guide star techniques such as ultrasound encoding are incorporated. Fluorescence imaging with high molecular specificity are enabled in high depths of biological tissue.

Because of the dynamic developments on this field, fast AO systems have become commercially available for applications requiring high temporal resolutions. This progress offers a great potential also for fluid flow research. The light propagation in flow measurement techniques requires undistorted optical paths in the fluid, but often this is not the case. Whereas static distortions caused e. g. by glass windows can easily be corrected by means of an appropriate pre-adjustment of the optics, this is no longer possible in the presence of dynamic, i.e. time-varying distortions. Such wavefront distortions appear in a huge variety of technical fluid dynamic applications. On the one hand, they are caused by inhomogeneous media. Typical examples are temperature gradients in combustions [18], pressure gradients at shock waves in compressible fluids [19] and concentration gradients in electrolysis cells [20] as well as in plasma processes [21]. On the other hand, distortions result from fluctuating interfaces between two media of different optical density. Typical examples

are water channels with an open surface [22], multi-phase flows [23], blood flows, levitated droplets and flows alongside a phase boundary.

However, so far AO has been used in technical flow measurement methods only at very rare intervals. The objective of this contribution is to demonstrate that AO is an appropriate tool to improve the features of flow velocity measurement techniques in complex environments. To this end, the optical distortion of a fluctuating water surface wave is investigated regarding measurements by laser Doppler velocimetry (LDV). The technical relevance of this experiment is given by film flows, i.e. fluids of small thickness running down an inclined substrate with an open surface [24, 25]. Since film flows exhibit a high surface-to-volume ratio they are characterized by a high heat and mass transport. Consequently, film flows are widespread in industrial applications especially for chemical process engineering, e. g. for film-cooling, cleaning, evaporation, condensation and distillation, to name a few.

## 2. Preliminary considerations

### 2.1 Velocity measurement technique

One of the most often applied velocity measurement technique for fluid flow research is laser Doppler velocimetry (LDV). The principle is based on a Mach-Zehnder interferometer. Two coherent Gaussian laser beams are made to intersect under a small angle  $\theta$ , the half angle between the beams. In the intersection area, i.e. the measurement volume, an interference fringe system is generated. Typically the fluid is seeded by small tracer particles, following the flow with negligible slip. Tracer particles passing the measurement volume generate scattered light which interferes at a photodetector. The flow velocity is determined by the measured Doppler frequency  $f_D$  of the interference signal and the fringe spacing  $d$ :  $v = f_D \cdot d$ . The fringe spacing is expressed by [26]

$$d(z) = \frac{\lambda}{2 \sin \theta} \left[ 1 + \frac{z \cos^2 \theta (z \cos^2 \theta - z_w)}{z_R^2 \cos^2 \theta - z_w (z \cos^2 \theta - z_w)} \right], \quad (1)$$

with  $\lambda$  as the light wavelength,  $z$  as the longitudinal coordinate and  $z_w$  as the position of the beam waists with respect to the position of the beam intersection. The Rayleigh length  $z_R$  characterises the optical wave fronts and is defined by  $z_R = \pi w_0^2 / \lambda$ , where  $w_0$  is the radius of the beam waist.

It gets obvious that the fringe spacing  $d$  is strongly affected by the intersection angle  $\theta$  of the beams as well as by the laser beam parameters such as the radius  $w_0$  and position  $z_w$  of the beam waists. A variation of  $d$  enhances the measurement uncertainty of the flow velocity [27]. Consequently, the laser beam parameters have to be stabilized against occurring optical distortions, e.g. caused by a fluctuating air-water interface.

### 2.2 Consideration of the optical distortions

**Table 1. Classification of the optical distortions caused by the fluctuating air-water interface.**

Order	Phenomenon of the interface	Effect	Correction by
0	Stroke / amplitude	Dislocation of the measurement volume	Mirror stroke
1	Tilt	Dislocation of the measurement volume, change of fringe spacing	Mirror tilt
2	Curvature	Change of beam waist position / defocus	Mirror curvature
$\geq 3$	Distortion	Distortions of the fringe systems	Individual setting of mirror elements

In order to estimate the variation of the LDV measurement properties caused by the optical distortion, the height function  $h(x,t)$  of the air-water interface is developed into a Taylor series. For a simplification, only the one-dimensional expression is considered here:

$$h(x,t) = \underbrace{h(x_0,t)}_{\text{Stroke}} + (x-x_0) \underbrace{\left. \frac{\partial h(x,t)}{\partial x} \right|_{x=x_0}}_{\text{Tilt}} + \frac{1}{2} (x-x_0)^2 \underbrace{\left. \frac{\partial^2 h(x,t)}{\partial x^2} \right|_{x=x_0}}_{\text{Curvature}} + \dots, \quad (2)$$

with  $x_0$  as the incident position of the laser beam. The consequences for the measurement properties are discussed for the orders of the derivate of the height function  $h(x,t)$ , see also Table 1:

*0th order: Stroke, i.e. height of the interface.* Ray optics: For a lift of the interface a parallel shift of the beam occurs whereas the beam direction remains constant. The consequence is a shift of the measurement volume, i.e. a dislocation of the measurement position. Wave Optics: As the air-water interface performs a random movement with time, a stochastic imbalance of the Mach-Zehnder interferometer results, see Fig. 1. The occurring

phase jitter disturbs the interference signal frequency:  $f = \frac{v}{d} + \frac{n_W - n_A}{\lambda} \cdot \dot{h}$ ,  $\dot{h} = \left. \frac{dh}{dt} \right|_{x=x_0}$ ,

where  $\dot{h}$  is the vertical velocity of the moving water surface.  $n_W$  and  $n_A$  are the refractive indices of the water and air, respectively. The first term describes the standard laser Doppler frequency whereas the second term represents the contribution of the phase jitter caused by the rising water surface.

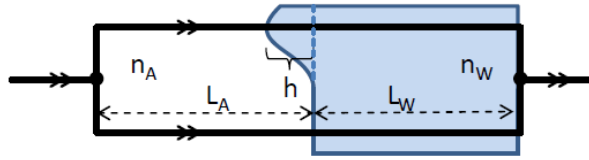


Fig. 1. Sketch of the Mach-Zehnder interferometer setup of an LDV which is partly submerged in water ( $h$ : height of the water wave,  $n_A$ : air refractive index,  $n_W$ : water refractive index,  $L_A$ : geometrical path length in air,  $L_W$ : geometrical path length in water).

*1st order: Tilt of the interface.* Due to refraction, a tilt of the interface will change the propagation direction of the beam. Going to the two-dimensional consideration, it has to be distinguished between a tilt in the plane spanned by the two partial beams  $\delta_x$  and a tilt in the direction normal to this plane  $\delta_y$ . *Tilt in x-direction (tip):* A change of the beam direction will result in a different position of the beam crossing, i.e. again a dislocation of the measurement position. Moreover, it will lead to different crossing angles  $\theta$ , to a different fringe spacing  $d$  according to Eq. (1) and to an enhanced velocity measurement uncertainty. *Tilt in y-direction:* A beam deflection in the  $y$ -direction normal to the plane spanned by the two Gaussian beams will result in skew rays. The reduced overlap of the partial beams results in lower rate of valid LDV signals, i.e. a reduced measurement time. In the worst case of negligible beam overlapping no measurements can be performed at all.

*2nd order: Curvature of the interface.* Due to refraction, a curvature of the interface induces a lens effect on the beam propagation. It changes the radius  $w_0$  and the position  $z_B$  of the beam waist. As a consequence, the fringe spacing  $d$  is changed according to Eq. (2), which enhances the velocity measurement uncertainty [27].

*3rd order and higher orders: Distortions of the surface with high spatial frequency.* The wavefront of the beams will be locally distorted, leading to inhomogeneities in the interference fringes. The fringe spacing can vary in all three directions  $d = d(x,y,z)$ . In consequence the measurement uncertainty will increase.

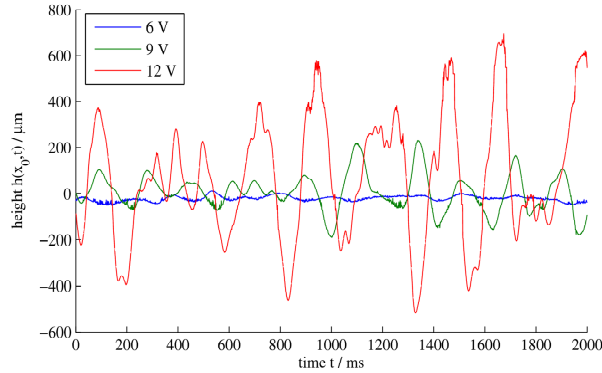
It should be noted that the extent, at which the different distortion orders appear, strongly depend on the incidence point of the beam with respect to the surface wave, i.e. on the phase of the wave. For example, if the beam passes through a maximum of the water wave, a convergent lens will mainly affect the beam, if it passes through a minimum, a divergent lens effect appears. If the beam propagates through the zero-crossing of the wave, mainly a beam deflection and a phase jitter will occur.

### 3. Experiments

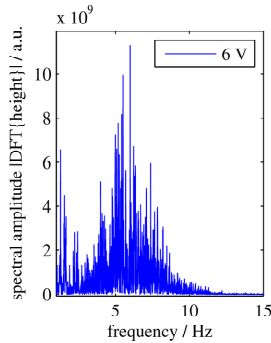
#### 3.1 Characterization of the distortion

In order to define the requirements for the AO system, the optical distortion of the fluctuating air-water interface has to be characterised. The fluctuation of the interface was generated by a water pump, see also the description of the experimental setup in the next section. Height measurements of the interface were conducted using a chromatic-confocal distance sensor (Micro Epsilon Optronic GmbH, Dresden, Germany) with a measurement rate of 1 kHz. This sensor principle is based on the spectroscopic evaluation of chromatic aberration. It turned out to be well suited for measuring the height of the reflecting water surface. The stroke, i.e. height  $h$  of the water surface was measured as a function of time for different operation voltages of the employed water pump. Figure 2(a) shows the results for three different voltages as an example and their corresponding Fourier spectra in Figs. 2(b)–2(d). As can be seen, the maximum frequency occurs at about 6 Hz and is almost independent of the pump voltage. The spectrum contains significant frequency contents until several tens of Hertz.

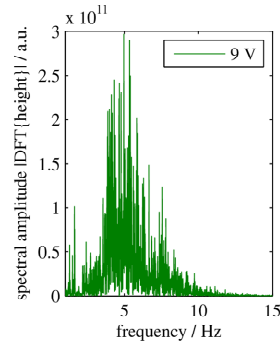
(a)



(b)



(c)



(d)

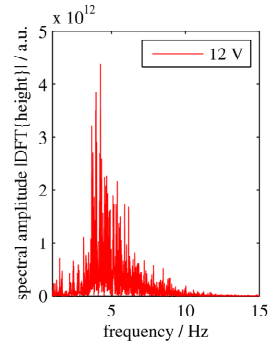


Fig. 2. Characterisation of the water surface fluctuations for three different operation voltages of the pump. (a) Time signals and (b)-(d) corresponding spectra.

The phase velocity  $v_{ph} = \omega / k$  and the wavelength of the surface waves can be deduced from the dispersion relation for water waves [28]:  $\omega^2 = \tan h(h_0 k) \left( \frac{\sigma k^3}{\rho} + gk \right)$ , where  $\omega = 2\pi f$  is the angular frequency and  $k = 2\pi/\lambda$  the angular wave number of the water wave,  $\sigma = 72 \cdot 10^{-3} \text{ kg/s}^2$  the air-water surface tension,  $\rho = 1 \cdot 10^3 \text{ kg/m}^3$  the water density,  $g = 9.81 \text{ m/s}^2$  the gravitational acceleration and  $h_0 = 5.2 \text{ cm}$  the absolute water height above the bottom of the basin. Considering the maximum frequency of 6 Hz yields a phase velocity of 0.3 m/s and a wave wavelength of 50 mm. Hence, the water waves can be allocated mainly to the capillary wave regime.

Based on these characterizations of the air-water interface the requirements for the AO system can be deduced. In general, an AO system consists of three components [29], a wavefront sensor (e.g. a Hartmann-Shack camera), an adaptive optical element (e.g. a deformable or segmented mirror) and a control unit that reads the wavefront data and calculates the control parameters for the adaptive element. The AO system represents a closed-loop feedforward-control for the distortions of the optical imaging system. In the following the necessary features of the components are outlined.

The maximum occurring frequency to be corrected is about 50 Hz. In accordance to the Nyquist-Shannon sampling theorem, the AO system should have a sampling rate of the controlling of at least 100 Hz. The wavelength of the capillary wave of about 50 mm is significantly larger than the laser beam diameter at the water surface of about 1 mm. Consequently, for the adaptive optical element a low number of actuators is sufficient since no high spatial frequencies need to be corrected. The required tilting range of the adaptive optical element can be estimated from the inclination of edge of the capillary wave using

$$\tan \delta = \frac{\partial h}{\partial x} = -\frac{1}{v_{ph}} \frac{\partial h}{\partial t}.$$

Negligible dispersion and a shape conservation of the capillary wave

were assumed. This yields a mean tilting angle of the water surface of  $\pm 24 \text{ mrad}$  for the highest pump voltage. Taking into account the angular magnification of the optical system of 0.033 (see section 3.2), yields a required tilting range of for the adaptive optical element of  $\pm 0.79 \text{ mrad}$ .

Under consideration of these specifications, an adaptive optics system from Flexible Optical B.V. (OKO tech) was chosen, which consists of a deformable membrane mirror (DM) with integrated tip-tilt stage, a Hartmann-Shack wavefront sensor (HS-WFS) and a controller based on a PC. The micromachined MOEMS deformable membrane mirror (DM) has a clear aperture of 10 mm and consists of 17 actuators that are driven electrostatically [30]. A modulation rate of 1 kHz and a maximum stroke of  $\sim 9 \mu\text{m}$  are obtained. A minimum focal length of approximately 3 m is resulting. The DM is mounted on a two-axis piezoelectric tip-tilt stage that allows angles of  $\pm 1.2 \text{ mrad}$  with a modulation frequency of 200 Hz. Typically 8x8 elements of the microlens array are used for the HS-WFS camera, exhibiting a frame rate of 400 Hz. The control software reads the wavefront data and drives the deformable mirror in closed-loop operation. The bandwidth of the whole feedback control is 200 Hz. It enables to compensate distortions with frequencies up to 100 Hz in accordance to the Nyquist-Shannon sampling theorem.

### 3.2 Experimental setup

Employing a solid state laser of 532 nm wavelength, an LDV has been realized, see Fig. 3. A prism beam splitter generates the two partial beams. The partial beams propagate through beam conditioning lenses, are directed downwards onto a water-filled basin and made to intersect by two separate mirrors  $M_2$  and  $M_3$ . For this experiment, the dynamic air-water interface will represent the optical distortion. In order to generate surface waves of stochastic behaviour and to avoid standing waves, a water pump was chosen to generate a flow in the basin. For the fundamental investigations intended here it is sufficient that only one beam is affected by the distortions and corrected by the AO system, see Fig. 3. One partial beam was

directed with  $M_1$  onto the deformable mirror DM. A small incident angle ( $\approx 10^\circ$ ) was chosen to avoid an elliptical beam deformation. After running through the basin the beam was split by a prism beam splitter whose reflected partial beam was directed onto the HS-WFS to measure the beam distortions caused by the fluctuating interface. The second partial beam of the first beam splitter was guided directly into the basin. A glass plate was fixed on the water surface at the beam incident point to prevent the distortion of this beam.

One challenge when using the DM is to keep the position of the beam intersection constant, i.e. that the incident point  $x_0$  of the beam has to be kept constant as well. If the DM would be applied as the last component above the water surface, then the tip-tilt function would deflect the beam to different incident positions. This problem was solved by inserting a Keplerian telescope ( $L_6 - L_7$ ) between the DM and the water surface such that the DM is located in the focal plane of the first lens  $L_6$  and the water surface in the focal plane of the second lens  $L_7$ . If the interface exhibits a certain angle  $\delta = \arctan(\partial h / \partial x)|_{x=x_0}$  with respect to the horizontal, then the beam deflection in water due to refraction can be compensated by changing the incident angle by an angle  $2\kappa$ , which is attained by a mirror tilt of angle  $\kappa$  approximately given by:  $\kappa = -\frac{f_2}{f_1} \frac{n_w - n_A}{n_A} \frac{\delta}{2}$ , where  $f_1$  and  $f_2$  are the focal lengths of the first ( $L_6$ ) and the second lens ( $L_7$ ) of the Keplerian telescope, respectively. Hence, the Keplerian telescope can be dimensioned that the tilting range is magnified. In the experiment,  $f_1 = 300$  mm and  $f_2 = 60$  mm yielding  $\kappa \approx 0.033 \delta$ .

The beam intersection (i.e. the measurement volume) was adjusted to be located underneath the basin. An optical chopper (OC) with a fixed pinhole (PH) as scattering object was arranged in the measurement volume. The chopper rotates with constant circumferential speed and acts as a velocity normal for the experiments.

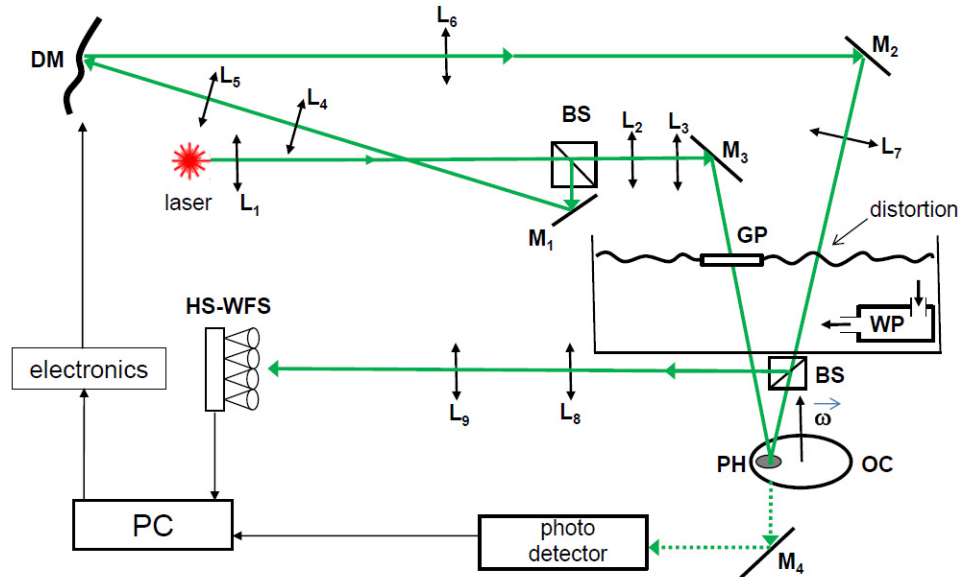


Fig. 3. Experimental setup: Laser Doppler velocimeter with adaptive optics system implemented in one partial beam to correct for wavefront distortions. M: mirror, L: lens, BS: prism beam splitter, GP: glass plate, PH: pinhole, OC: optical chopper, HS-WFS: Hartmann-Shack wavefront sensor, DM: deformable mirror, WP: water pump, PC: personal computer.

### 3.3 Results

Since the distortions are of random nature, a characterisation of the measurement properties and the assessment of the wavefront correction by the AO system have to be performed by means of statistical evaluations. The interference contrast, the validation rate and the velocity measurement uncertainty can be considered figures of merit of the LDV system. As derived from the considerations in section 2.1, the appearance of skewed rays will affect the beam overlap. It is expressed in the visibility of the interference signal

$$V = \frac{I_{\max} - I_{\min}}{I_{\max} + I_{\min}} \quad (3)$$

with  $I_{\max}$  and  $I_{\min}$  as the maximum and minimum intensities of the modulation signal. A poor modulation degree will also result in a low signal-to-noise ratio (SNR). In LDV systems an SNR threshold is used as one validation criterion usually. The validation rate, i.e. the ratio of valid LDV signals with sufficient modulation degree to the total number of LDV signals, is used as a measure for a fully-developed interference fringe system as well.

In the experiment, 1000 LDV burst signals were recorded for each voltage setting of the water pump and also for the non-fluctuating interface at rest, i.e. a water pump voltage of 0 V. The results for the mean interference contrast and the mean validation rate are shown in Figs. 4(a) and 4(b) as a function of the distortion amplitude, respectively. The interference contrast for the non-disturbed water surface at rest is about 83%, see Fig. 4(a). It decreases monotonically with increasing amplitude of the distortion to about 8% for the highest average wave height of  $\sim 220 \mu\text{m}$ . If the AO system is activated, the interference contrast is improved over the whole amplitude range. The maximum improvement occurs at medium distortion amplitudes, where the interference contrast rises from 22% to 48%. A similar behaviour can be seen at the validation rate which is displayed in Fig. 4(b). It decreases from 100% for the undistorted case exponentially to about 8% for the highest distortion amplitude. With the wavefront correction by AO applied, the validation rate is improved over the whole range. The maximum improvement occurs for moderate distortion amplitudes. An enhancement of 50% is achieved for distortion amplitude of about  $50 \mu\text{m}$ . Higher distortion amplitudes are more difficult to compensate by the current AO system. The reasons are discussed in the next section.

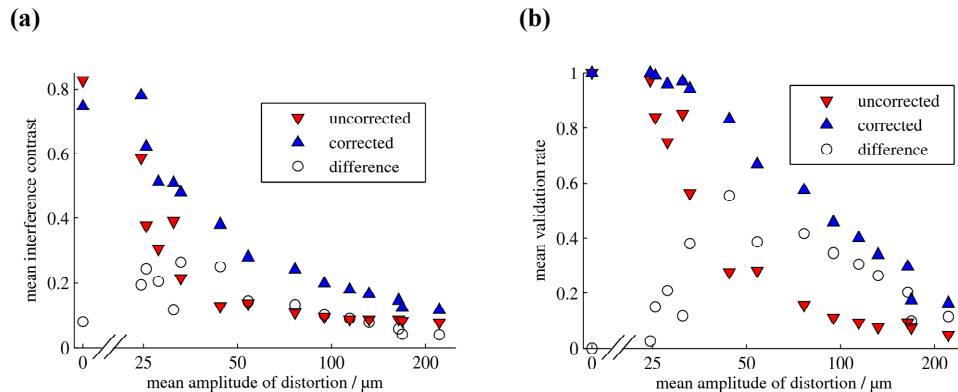


Fig. 4. Interference contrast (a) and rate of valid LDV signals (b) at threshold of 10% interference contrast in dependence of the mean amplitude (stroke) of the interface distortion.

Moreover, the velocity measurement uncertainty has been studied. The velocity of the rotating pinhole as scattering object is controlled to a constant value in order to calculate the measurement uncertainty. The relative standard deviation rises up to about 2.5% at the maximum distortion amplitude of  $220 \mu\text{m}$ . With the active AO system the relative uncertainty

was reduced over the whole range. However, the improvement is the better the smaller the amplitudes are. At distortion amplitudes smaller than 25  $\mu\text{m}$  the measurement uncertainty is reduced with the AO correction by more than a factor of two to an uncertainty of about 1%. In the next section these results are discussed based on a numerical simulation.

#### 4. Simulation

In order to estimate the individual contributions of the different effects in section 2.2 to the measurement uncertainty and the validation rate, a numeric simulation of the measurement process has been performed. A series of 1000 LDV signals per pump voltage was simulated, using the measured amplitude-time function of the water surface. Calculating the interference fringe systems is done by solving the Helmholtz equation. This quasi-stationary approach can be used because the frequency of the surface wave is negligibly small compared to the frequency of light. The refractive index field is defined by piecewise homogeneous media. For the propagation of light in homogeneous media the wave propagation method (WPM) [31] is used. The propagation equation is  $U(x, y, z_1) = F^{-1} \{ F \{ U(x, y, z_0) \} \exp(-ik_z(z_1 - z_0)) \}$ , where  $U$  denotes the complex amplitude of the scalar electrical or magnetic field of light.  $z = z_0$  is the start plane and  $z = z_1$  is the end plane for the propagation. The Fourier transform  $F$  and its inverse  $F^{-1}$  refer to  $(x, y)$  and  $(k_x, k_y)$ , respectively, and the  $z$ -component of the wave vector is given by

$$k_z = \sqrt{\left(\frac{2\pi n}{\lambda}\right)^2 - k_x^2 - k_y^2} \quad (4)$$

with the wavelength  $\lambda$  and the refractive index  $n$ . As long as  $n$  stays constant, there are no limitations in step size  $z_1 - z_0$  along the optical axis, which allows for fast calculations. Since the WPM is based on Fourier transform, it can be easily combined with a three-dimensional Fourier space rotation of a light field [32]. The light field rotation is necessary because the angle of the water surface is changing, and therefore we need to calculate the electromagnetic field of the laser beam in arbitrary tilted planes. In the plane of the phase transition at the air-water interface Snell's law can then be applied for every single decomposed plane wave by inserting the actual refractive index  $n$  into Eq. (4). Additionally to the tilt of the water surface, the local curvature is considered by an approximation through a thin lens:  $U(x, y, z_1) \approx U(x, y, z_0) \exp(i2\pi \Delta(x, y)/\lambda)$ . The spatial varying optical path length  $\Delta(x, y)$  is modelled as a parabola with the local curvature  $\partial^2 h / \partial x^2$  of the water surface.

**Table 2. Steps of the simulation for calculating one interference fringe system.**

#	Operation
1	propagation in air ( $n = 1$ ) until the height of the interface $h(x_0, t)$
2	transmission through thin lens with curvature given by $\partial^2 h / \partial x^2$
3	tilting by an angle $\delta = \arctan(\partial h / \partial x)$
4	phase transition from $n = 1$ to $n = 1.33$
5	propagation in water ( $n = 1.33$ ) until the depth of the measurement volume
6	summation with the light field of the second (undistorted) beam
7	calculation of the intensity as the square of the absolute value

A summary of all steps for calculating one interference fringe system is shown in Table 2. The light field of the first step is calculated from the measured beam profile at the measurement volume by accomplishing the whole procedure backwards.

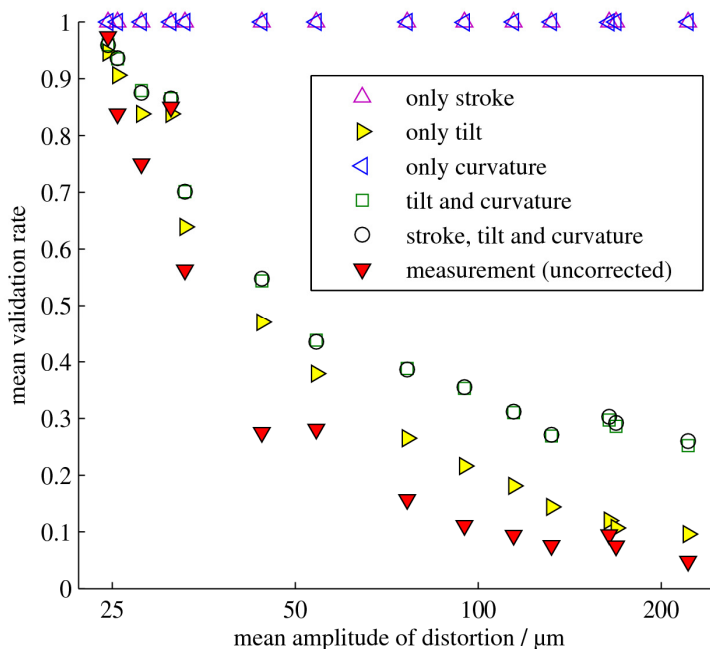


Fig. 5. Comparison of the measured and simulated mean validation rate in dependence of the mean amplitude of the water surface wave, i.e. the distortion. Three different orders of the Taylor series development of the surface height function are considered in the simulation.

The simulated budget of the validation rate is shown in Fig. 5. According to Table 1 and Eq. (2) the different orders of the Taylor series development of the water surface wave are discussed based on the parameters of the employed AO system. The single contribution of the stroke and the curvature can be neglected. In contrast, the tilting angle of the piezo actuator exhibits the major budget term of the validation rate, see Fig. 5. Too large amplitudes of the distortion cannot be corrected, resulting in skewed laser beams. They reduce the interference visibility, see Eq. (3), the validation rate of the LDV signals and the available measurement time. In consequence, the tilting angle of the deformable mirror of the AO system has to be increased, if higher distortion amplitudes should be corrected. Figure 5 also shows the covariance between the curvature and the tilt, i.e. the stroke. This correlation coefficient has to be regarded for the dimensioning of an optimized AO system.

From the simulation also the budget of the velocity measurement uncertainty can be investigated. The single contribution of stroke and tilt does not contribute much to the total uncertainty. Also the phase jitter caused by the rising water surface (see Fig. 1) is not dominating over the other effects. This is an important finding since the AO system is not able to compensate the phase jitter. The main budget contribution to velocity measurement uncertainty occurs, if tilt and curvature appear concurrently. A significant covariance between tilt and curvature occurs. Moreover, it is estimated that curvature attainable with the employed deformable mirror is not sufficient to compensate the lens effect of the water surface. The implementation of an adaptive lens would overcome this problem since offers a larger tunable range of the focal length.

## 5. Conclusion

The experiments revealed that adaptive optics (AO) is an appropriate tool to improve the properties of fluid flow measurement techniques in complex environments. In this contribution we have performed a fundamental analysis of the effects of wavefront distortions on the velocity measurement properties of a Mach-Zehnder interferometer. The optical

distortion is caused by a dynamic air-water interface. The investigations confirmed that the measurement properties can be improved for all amplitudes of the distortions when using the AO system. At a mean water wave amplitude of about 50  $\mu\text{m}$  the validation rate was raised from 28% without correction to about 83% with correction by the AO system. A numeric simulation revealed the necessary parameters of an optimized AO system in order to eliminate the optical distortions also for higher water wave amplitudes. To allow for measurements with an optical access only from one side, the Fresnel reflex can be used for wavefront sensing instead of the transmitted beam. In summary, the rapid progress of the AO components will allow flow measurements in situations that were hardly accessible before.

### **Acknowledgments**

Dr. Oleg Soloviev and Dr. Seva Patlan from Flexible Optical B.V. (OKO tech, GG Rijswijk ZH, The Netherlands) are thanked for their support on the AO system. Prof. Roland Sauerbrey (Helmholtz-Zentrum Dresden-Rossendorf, Germany) is thanked for fruitful discussions.